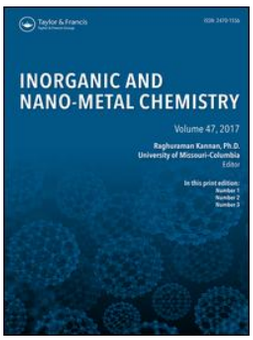

Inorganic and Nano-Metal Chemistry

ISSN: 2470-1556 (Print) 2470-1564 (Online) Journal homepage: http://www.tandfonline.com/loi/lsrt21

Electrical and magnetic properties of Cd^{+2} doped Ni-Zn ferrites

M. R. Patil, M. K. Rendale, S. N. Mathad & R. B. Pujar

To cite this article: M. R. Patil, M. K. Rendale, S. N. Mathad & R. B. Pujar (2017) Electrical and magnetic properties of Cd^{+2} doped Ni-Zn ferrites, Inorganic and Nano-Metal Chemistry, 47:8, 1145-1149, DOI: 10.1080/24701556.2017.1284097

To link to this article: http://dx.doi.org/10.1080/24701556.2017.1284097

Accepted author version posted online: 26 Jan 2017.
Published online: 26 Jan 2017.

INORGANIC AND NANO-METAL CHEMISTRY
2017, VOL. 47, NO. 8, 1145–1149
http://dx.doi.org/10.1080/24701556.2017.1284097

Taylor & Francis
Taylor & Francis Group

Electrical and magnetic properties of Cd^{+2} doped Ni-Zn ferrites

M. R. Patil[a], M. K. Rendale[b], S. N. Mathad[c], and R. B. Pujar[a,d]

[a]S.S. Arts College, T.P. Science Institute, Sankeshwar, India; [b]Department of Engineering Physics, K.L.S. Gogte Institute of Technology, Belagavi, India; [c]Department of Engineering Physics, K.L.E. Institute of Technology, Hubli, India; [d]Department of Physics, P.C. Jabin Science College, Hubli, India

ABSTRACT

This article reports synthesis, electrical, and magnetic properties of $Ni_{0.5-x}Cd_xZn_{0.5}Fe_2O_4$ (with X = 0.0, 0.15, 0.30, and 0.45) ceramics by simple solid state method. The temperature dependence of the electrical conductivity plot shows the semiconducting behavior, which can be attributed to ferromagnetic-paramagnetic transition. The activation energies obtained from resistivity plots in paramagnetic region is witnessed to be more than that in ferri-magnetic region. The conduction mechanism in nickel-zinc (Ni-Zn) ferrite particles has been discussed on the basis of hopping of electrons. The magnetic hysteresis at room temperature indicates the ferri-magnetic behavior of synthesized ferrite system. The detailed influence of cadmium doping in Ni-Zn ferrites found to be enhances saturation magnetization, remnant magnetization, coercivity, magnetic moment, and Y-K angles.

ARTICLE HISTORY
Received 16 June 2016
Accepted 16 January 2017

KEYWORDS
Ni-Zn ferrites; electrical properties; activation energy; magnetic moment; Y-K angle

Introduction

There is an increasing interest in ferrite magnetic materials because of their broad applications in legion technological disciplines viewing ferrofluids, information storage, and drug delivery.[1] Ferrites are technologically substantive materials that are used in the fabrication of electronic, microwave, and magnetic devices. Because their high resistivity and negligible eddy current losses, they have gained technological importance.[2,3] Ni-Zn ferrite is of greater commercial application in the electromagnetic interfaces known as EMI, which is used in hard disk drives, laptops, and other electronic products.[4] The outstanding combinational properties like high electrical resistivity, high permeability, compositional stability, and low eddy current losses attracted researchers due to their potential applications in diverse fields.[5] The properties of Ni-Zn ferrites can be castrated by changing preparation methods (like solid state method, sol-gel method, co-precipitation method, etc.), chemical composition, sintering temperature, and impurity element. Elemental structural properties of nickel-zinc ferrites have been studied by Refs.[5–8] The dielectric properties[9] and magnetic properties of Ni-Zn ferrites were reported.[7] Researchers have also shown interest in the structural, electrical, and dielectric properties of doped Ni-Zn ferrite. Influence of calcium oxide and silicon oxide doping,[10] MnO2 doped,[11] copper doped,[12] Sm^{+3} doped[13] in Ni-Zn ferrites has been reported. There are several methods[5–14] of synthesis like solid state method, sol-gel methods, chemical method, double sintering ceramic technique, hydrothermal methods, and co-precipitation method.[5–14]

However, the literature survey on $Ni_{0.5-x}Cd_xZn_{0.5}Fe_2O_4$ ferrites indicates that not much work has been done. Focusing on these objectives we have prepared, in the present work standard double sintering ceramic route was used to synthesize the polycrystalline $Ni_{0.5-x}Cd_xZn_{0.5}Fe_2O_4$ ferrite .This method is easier and cheaper for fabrication of the materials is as compared to other methods in addition, the grain size and sintering temperatures are easily controllable. The present work is engrossed on the study of electric and magnetic properties of cadmium substituted nickel-zinc ferrites.

Experimental

In agate mortar (in acetone medium), high purity nickel oxide, cadmium oxide, zinc oxide, and iron oxide were mixed in stoichiometric proportion to obtain the desired compound ($Ni_{0.5-x}Cd_xZn_{0.5}Fe_2O_4$). All samples were pre-sintered at 800°C for 10 h. Powders were subjected to hard milling in acetone medium and dried powders were sieved to obviate the large sized particles. Using hydraulic press (pressure of ten tons for 5 min) pellets were prepared to obtain dense pellets. Final sintering is done at 1000°C by keeping them on an alumina sheet in a silicon carbide furnace for 20 h to enable complete solid state reaction.[14] The DC electrical resistance for all compositions was measured by two-probe methodology applying silver conductor paste on each side, and the room temperature to well beyond the Curie temperature. The sample holder was then placed in temperature regulated furnace provided with thermocouple. The schematic flow chart of the process is shown in Figure 1.

The resistivity ρ was calculated using the relation:

$$\rho = \frac{\pi r^2 R}{t} \quad (1)$$

where t = thickness of pellet in cm. r = radius of the pellet in cm. R = resistance in ohm.

CONTACT S. N. Mathad physicssiddu@gmail.com Department of Engineering Physics, K.L.E. Institute of Technology, Hubli 580030, India.
Color versions of one or more of the figures in the article can be found online at www.tandfonline.com/lsrt.

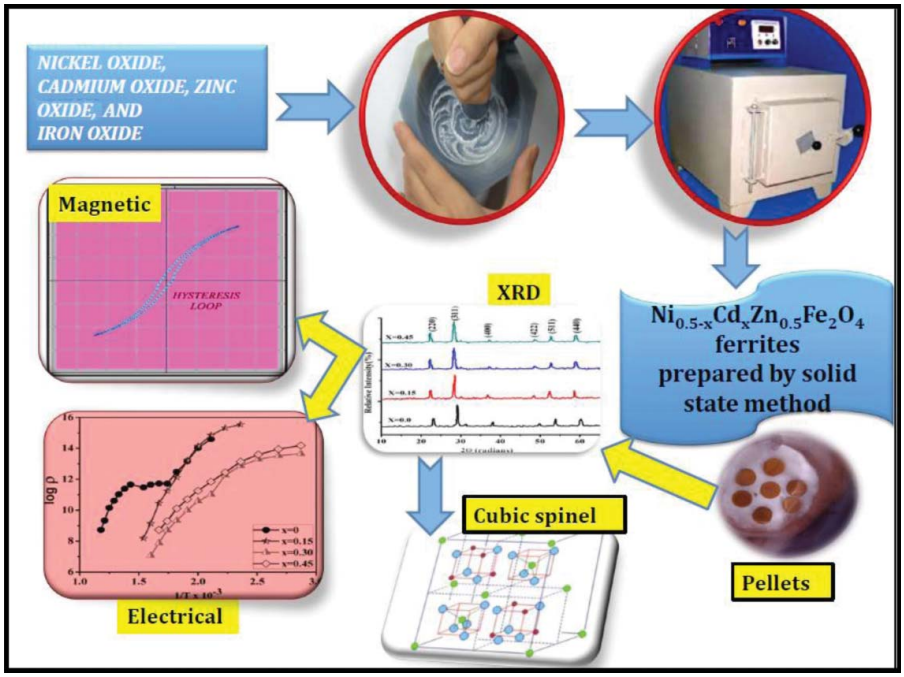

Figure 1. Schematic flow chart of the proposed work.

The activation energy was calculated using the equation:[19]

$$E = 2.303\ K \text{ slope of } \log \rho \text{ vs. } (1000/T) \text{ curve} \quad (2)$$

The room temperature magnetic measurements for all the compositions were performed by using a computerized high field hysteresis loop tracer (Magenta, Mumbai) at 5 kOe magnetic field strength. The ferromagnetic B–H hysteresis loop parameters such as saturation magnetization (Ms), coercive field (Hc), and retentivity (Mr) were measured from the observed B–H loop, recorded by using high field hysteresis loop tracer. The magnetic moment per formula unit in Bohr magneton (n_B) was calculated by using the following relation:[20]

$$n_B = \frac{M \times M_S}{5585} \quad (3)$$

where M is the molecular weight and Ms is the saturation magnetization per gram of the sample.

The Y–K angles of ferrite samples were estimated using the following relation:[4]

$$\cos\alpha_{yk} = \frac{n_B + 5(1-x)}{7(1+x)} \quad (4)$$

where n_B is the Bohr magneton, x is the concentration of substituted ion.

Structural studies

X-ray diffraction patterns of $Ni_{0.5-x}Cd_xZn_{0.5}Fe_2O_4$ (X = 0.0, 0.15, 0.30, and 0.45) ferrites are shown in Figure 2. According to it, the planes that diffract X-rays are (220), (311), (400), (422), (511), and (440). All the samples exhibit cubic spinel structure. The absence of extra lines in the patterns confirms the formation of single phase ferrites. Interplaner spacing and lattice parameter (a) were calculated and tabulated in Table 1.

$$d = \frac{a}{(h^2 + k^2 + l^2)^{1/2}} \quad (5)$$

Electrical studies

The plots shown in Figure 3 of log ρ vs 1000/T for $Ni_{0.5-x}Cd_xZn_{0.5}Fe_2O_4$ (where x = 0, 0.15, 0.3, and 0.45) are negative temperature coefficient (NTC) behavior of the material. These plots show transition near Curie temperature. At this temperature the material changes from ferromagnetic state to paramagnetic state. The change in slope is observed in all the ferrites in two regions. The activation energy corresponding to paramagnetic and ferromagnetic regions are calculated from the plot of log ρ vs 1000/T. The data on activation energy, Curie temperature, are given in Table 2. It is evident from the

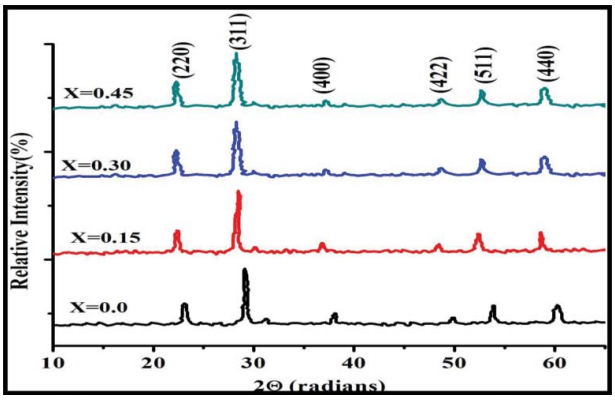

Figure 2. XRD patterns of $Ni_{0.5-x}Cd_xZn_{0.5}Fe_2O_4$ (X = 0.0,0.15,0.30, and 0.45).

Table 1. Interplaner spacing(d) and lattice parameter (a) of ferrites.

X = 0.0 a = 8.3747 A°		X = 0.15 a = 8.4157 A°		X = 0.30 a = 8.5082 A°		X = 0.45 a = 8.4593 A°	
d_{obs}, A°	d_{cal}, A°	d_{obs}, A°	d_{cal}, A°	d_{obs}, A°	d_{cal}, A°	d_{obs}, A°	d_{cal}, A°
2.9570	2.9592	2.9795	2.9795	4.8517	4.8518	2.5751	2.5751
2.5231	2.4740	2.5422	2.5422	2.5633	2.5633	2.4678	2.4678
2.0931	2.0523	2.1082	2.1082	2.1212	2.1212	1.7440	1.7440
1.7094	1.6761	1.7007	1.7007	1.7331	1.7331	1.6447	1.6447
1.6131	1.5817	1.6226	1.6226	1.6110	1.6110	1.3042	1.3042
1.4820	1.4531	1.4917	1.4917	1.2974	1.2975	1.1128	1.1128

table that activation energy in paramagnetic region is greater than that in ferromagnetic region. This result is in agreement with the theory of Irkhin and Turov.[15] The electrical conductivity in Li-Ni ferrites has been studied by Reddy et al.[16] They observed a transition at Curie temperature. Whall et al.[17] and Ahmed et al.[18] had remarked discontinuities in mixed nickel ferrites. Song et al.[19] had studied Co-Li ferrites and observed two regions of different slopes. They attributed the change in slope to the change in conduction mechanism. They have attributed the conduction mechanism to the electron hopping between Fe^{2+} and Fe^{2+} ions on the octahedral sites in the region of low activation energy. Smit and Wijn[20] had attributed the change in slope to the two parallel conduction mechanisms with different activation energies. The conduction in ferrites is primarily due to hopping of electrons from Fe^{2+} to Fe^{3+} ions on a crystallographically-equivalent site i.e. B site. The lowering of activation energy is attributed to the effect of spin ordering.[21] In the material, the decrease in the number of Fe^{3+} ions hinders the conduction mechanism. This leads to increase in the resistivity of the material as a consequence of increase in composition(x). In other words change in slope at Curie temperature is mainly due to spin ordering of electrons. The electrical conductivity of ferrites can be explained on the basis of the Verwey and de Boer mechanism[22,23] which involves the exchange of charge carriers, that is, electrons between the ions of the same element that are present in more than one valence state (Fe^{+2}, Fe^{+3}), distributed randomly over the crystallographic lattice sites.[24] This change in slope occurs while crossing the Curie temperature (the temperature at which the ferromagnetic material changed to paramagnetic).The

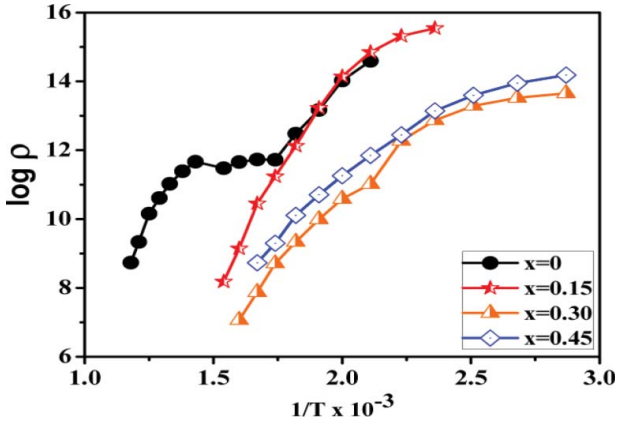

Figure 3. Variation of electrical conductivity with temperature of $Ni_{0.5-x}Cd_xZn_{0.5}Fe_2O_4$.

Table 2. Data on activation energy and Curie temperature for $Ni_{0.5-x}$ Cd_x $Zn_{0.5}$ Fe_2O_4 ferrites.

Cadmium content x	Curie temperature Tc (°C)	Activation energy, ferro region (Ea) (eV)	Activation energy, para region (eV)
X = 0	525	0.2117	0.3935
X = 0.15	325	0.1982	0.3726
X = 0.30	300	0.1501	0.2379
X = 0.45	275	0.1269	0.2027

discontinuity at the Curie temperature was attributed to the magnetic transition from well-ordered ferromagnetic state to disordered paramagnetic state which involves different activation energies. The values of the electrical resistivity (ρ) and thermal activation energies (E_a) of the prepared samples at ferromagnetic region and paramagnetic region were described in Table 2. It is also observed that the activation energy (E_a) in the ferromagnetic region is smaller than the paramagnetic region; this is due to the effect of spin disordering.[25] We know that from thermodynamics the magnetic transition is a second order transition and is accompanied by an expansive change in volume.[26,27] The decrease in DC resistivity with increase in Cd content up to 0.15 can be attributed to the excess formation of Fe^{2+} ions, since these ions may also be formed due to evaporation of cadmium during sintering process. The increase in resistivity with Cd content is attributed to the microstructure. Venugopal Reddy et al.[28] had reported the activation energy (E_a) for Li-Ni ferrite in ferromagnetic region in the range of 0.46–0.83 eV[25] and Ni-Cd ferrites in the range of 0.21–0.4 eV.[29]

The activation energy (E_a) lies in the range of 0.46–0.90 eV in ferromagnetic region for Ni-Cd ferrites.[30] For electron hopping the activation energy is found to be less than 0.2 eV and greater than 0.2 eV for polarons hopping. In the present case, large value of activation energy ($\Delta E > 0.2$ eV) suggest that the conductivity is due to hopping of polorons. Verwey et al.[31,32] reported that the conductivity in ferrites is due to the simultaneous presence of both Fe^{2+} and Fe^{3+} ions on octahedral sites. The conductivity in ferrites was attributed to the hopping of electrons between Fe^{2+} and Fe^{3+} ions on octahedral sites. Prakash et al.[33] have studies Ti^{4+} substituted Ni-Zn ferrites and explained the conductivity on the basis of hopping mechanism. The electrical properties of ferrites are affected by the distribution of cations on A and B sites, magnetic and non-magnetic substances, the amount of Fe^{2+} ions present, sintering condition, and microstructure. The ferrites which contain iron in excess show n-type conduction and those with iron deficiency show p-type conduction. The electron interacts with the ions of the lattice creating a local deformation of the lattice. This tends to follow the electron as it moves through the lattice. The lattice deformation increases the effective mass of electron as it partially drags the ion along with it. This effect is more pronounced due to strong Coulomb interaction in ionic crystals such as ferrites. The combination of an electron and strain field is called as polaron. Therefore mobility of electrons decreases and becomes highly temperature dependent.

The Curie temperature obtained from resistivity data are given in Table 2. It can be seen from the table that Curie temperature (T_c) decreases with cadmium content. The Curie temperature (T_c) majorly depends upon the intensity (strength) of

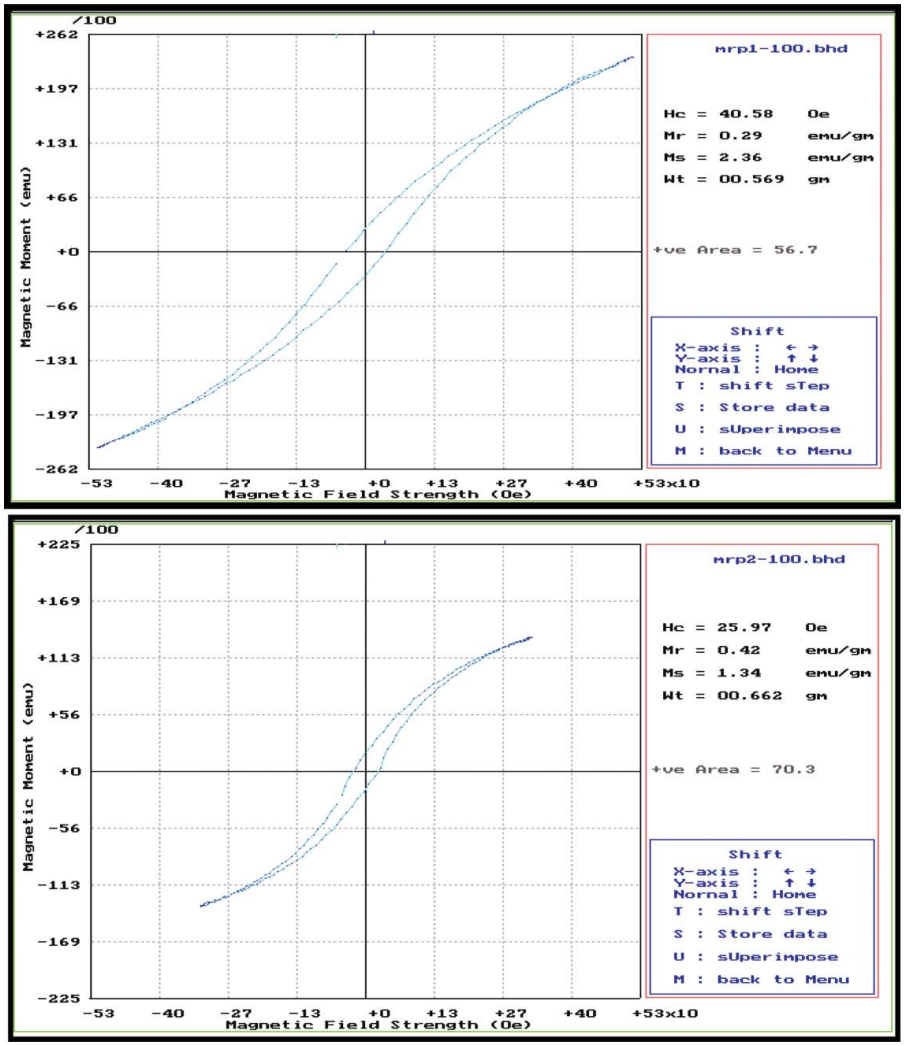

Figure 4. Magnetic hysteresis loops of $Ni_{0.5-x}Cd_xZn_{0.5}Fe_2O_4$.

A-B interaction. When non-magnetic ions are incorporated into lattice, the formation of co-ordination compounds such as Fe_A^{3+}-O^{2-} and Fe_B^{3+}-O^{2-}, on which T_c depends, decreases leading to the decrease in Curie temperature. The wide range of resistivity of ferrites is mainly explained on the basis of actual location of cations in the spinel structure and hopping mechanism. The high conductivity in ferrites is due to the simultaneous presence of both ferrous and ferric ions in the crystallographically-equivalent sites. The high resistivity in ferrites is associated with the occupation of B sites by divalent metal ions and trivalent iron ions. Such an arrangement requires a higher activation energy for hopping of electrons. The two mechanisms of conductivity can be represented as

$$Fe^{2+} + Fe^{3+} \leftrightarrow Fe^{3+} + Fe^{2+} + \Delta E$$
$$Me^{2+} + Fe^{3+} \leftrightarrow Me^{3+} + Fe^{2+} + \Delta E$$

Magnetic studies

The hysteresis loops for $Ni_{0.5-X}Cd_XZn_{0.5}Fe_2O_4$ samples (x = 0 and 0.15) are depicted in Figure 4. Magnetic parameters like Ms, Mr, and Hc are tabulated in Table 3. It is noticed that the saturation magnetization (M_s) decreases with increase in cadmium (Cd) content. As per the site preference energy, cadmium (Cd) ions occupy A site. As the amount of Cd on A site increases, more and more Fe^{3+} is replaced from A site to B site. The magnetic properties of ferrites depend on chemical composition, grain size, porosity, and interaction between tetrahedral and octahedral sites. In ferrites, the variation in saturation magnetization has been attributed to both surface spin effect and cation distribution on A and B sites.[32,33]

As the cobalt content increases in Ni-Cd ferrite, the inverse spinel Ni-Cd ferrite converts into mixed spinel ferrite. In the mixed spinel type structure, some nickel (Ni^{2+}) ions may occupy tetrahedral sites and hence the net magnetization found is relatively higher than that for inverse spinel structure. Prominent impact on the coercivity and saturation magnetization was observed due to cobalt ion doping which causes the pinning of the domain walls due to an increase in anisotropy.[32,33] This in turn affects the magnetic moment of an individual sublattice as

Table 3. Magnetic parameters for the $Ni_{0.5-x}Cd_xZn_{0.5}Fe_2O_4$ ferrites.

Cd Content	Ms	Hc	Mr/Ms	n_B	α_{yk}
0	2.36	40.50	0.228	0.101	43.22
0.15	1.34	25.97	0.313	0.06	47.32

well as A-B interaction. As a result A-B interaction gets weakened causing the decrease in saturation magnetization with increase in Cd content. At x = 0.3 and above B-B interaction becomes comparable in strength to A-B interaction. B spin becomes no longer parallel and net magnetization becomes zero.[34]

Conclusion

In summary, $Ni_{0.5-X}Cd_XZn_{0.5}Fe_2O_4$ ferrites were prepared by the solid state method. Temperature dependent DC electrical resistivity decreases with an increase in temperature ensuring the semiconductor-like nature. The variation of DC conductivity with temperature can be explained using the polaron hopping mechanism of electrons between the Fe^{+2} and Fe^{+3} due to their thermal activation. The activation energy calculated from the DC resistivity plots increases with an increase in cadmium content (x) in nickel-zinc ferrite. This activation energy may be attributed to the oxygen vacancy motion. Saturation magnetization, retentivity, coercivity, and magnetic moment are found to be decreasing with an increase in the cadmium content.

References

1. Ngo, A. T.; Pileni, M. P. *J. Phys. Chem. B* **2001**, *105*(1), 53–58.
2. Venkataraju, C.; Sathishkumar, G.; Sivakumar, K. *J. Magn. Magn. Mater.* **2010**, *322*(2), 230–233.
3. Goldman, A. *Modern Ferrite Technology*, Van Nostrand Reinhold: New York, **1990**.
4. Rama Krishna, K.; Vijaya Kumar, K.; Ravinder, D. *Adv. Mater. Phys. Chem.* **2012**, *2*, 185–191.
5. Ali, M. A.; Khan, M. N. I.; Chowdhury, F.-U.-Z.; Akhter, S.; Uddin, M. M. *J. Sci. Res.* **2015**, *7*, 65.
6. Kumar, A.; Annveer, Arora M.; Yadav, M. S.; Pant, R. P. *Phys. Proc.* **2010**, *9*, 20.
7. Prasad, M. S. R.; Prasad, B. B. V. S. V.; Rajesh, B.; Rao, K. H.; Ramesh, K. V. *J. Magn. Magn. Mater.* **2011**, *323*, 2115–2121.
8. Hashim, M.; Alimuddin, Kumar S.; Ali, S.; Koo, H. B.; Chung, H.; Kumar, R. *J. Alloy. Comp.* **2012**, *511*, 107.
9. Abdeen, A. M. *J. Magn. Magn. Mater.* **1999**, *192*(1), 121–129.77.
10. Hajalilou, A.; Hashim, M.; Ebrahimi-Kahrizsangi, R.; Sarami, N. *J. Phys. D: Appl. Phys.* **2015**, *48*, 145001.
11. Hua, S. U.; Zhang, H.-W.; Tang, X.-L.; Jing, Y.-L. *Trans. Nonferrous Metals Soc. China* **2011**, *21*(1), 109–113.
12. Barba, A.; Clausell, C.; Nuño, L.; Jarque, J. C. *J. Eur. Ceramic Soc.* **2017**, *37*(1), 169–177.
13. Liu, Z.; Peng, Z.; Lv, C.; Fu, X. *Ceramics Int.* **2017**, *43*(1), 1449–1454.
14. Patil, M. R.; Rendale, M. K.; Mathad, S. N.; Pujar, R. B. *Int. J. Self-Propagat. High Temp. Synth.* **2015**, *24*(4), 241–245.
15. Irkhin, Y. P.; Turov, E. A. *Sov. Phys. JEPT* **1957**, *33*, 673.
16. Venugopal Reddy, P.; Satyanarayana, R.; Seshagiri Rao, T. *Phys. Status Solidi* (a) **1983**, *78*, K 109.
17. Whall, T. E.; Young, K. K.; Prokova, Y. G. *Phill. Mag. B (GB)* **1986**, *54*, 505.
18. Ahmed, M. A.; El-Nimer, M. K.; Tawfik, A.; Hasab, A. M. *Phys. Status Solidi* (a) **1996**, *123*, 383.
19. Song, J. M.; Koh, J. G. *J. Magn. Magn. Mater* **1996**, *152*, 383.
20. Smit, J.; Wijn, H. P. J. *Ferriets*, John Wiley and Sons: New York, **1957**, p. 157.
21. Srinivasan, G.; Srivastava, C. M. *Phys. Stat. Solidi* **1981**, *108*, 665.
22. Verwey, E. J. W.; De Boer, F.; Van Santen, J. H. *J. Chem. Phys. Vet.* **1948**, *16*(12), 1091–1092.
23. Verwey, E. J. W.; de Boer, J. H. *Recueil des Travaux Chimiques des Pays-Bas* **1936**, *55*(6), 531–540.
24. El Hiti, M. A. *J. Magn. Magn. Mater.* **1994**, *136*, 138.
25. Aravind, G.; Ravinder, D.; Nathanial, V. *Phys. Res. Int.* **2014**, Article ID 672739, 11p.
26. Zemansky, M W. *Heat and Thermodynamics*, 6th ed., Mc Graw-Hill Book Company: New York, **1981**.
27. Yadav, S. P.; Shinde, S. S.; Kadam, A. A.; Rajpure, K. Y. *J. Semicond.* **2013**, *34*(9), 093002-1–093002-5.
28. Venugopal Reddy, P.; Seshagiri Rao, T. *J. Less Common Metals* **1981**, *79*, 191.
29. Devmunde, B. H.; Raut, A. V.; Birajdar, S. D.; Shukla, S. J.; Shengule, D. R.; Jadhav, K. M. *J. Nanoparticles* **2016**, Article ID 4709687, 8p.
30. Ashok, A.; Somaiah, T.; Ravinder, D.; Venkateshwarlu, C.; Reddy, C. S.; Rao, K. N.; Prasad, M. *World J. Condensed Matter Phys.* **2012**, *2*, 257–266.
31. Prakash, C.; Baijal, J. S. *J. Less Common Metals* **1985**, *106*, 257.
32. Patil, N. D.; Velhal, N. B.; Tarwar, N. L.; Puri, V. R. *Int. J. Eng. Innov. Technol.* **2014**, *3*(8), 73–77.
33. Hakim, M. A.; Nath, S. K.; Sikder, S. S.; Maria, K. H. *J. Phys. Chem. Solids* **2013**, *74*, 1316.
34. Kamble, P. N.; Vaingankar, A. S. *Indian J. Pure Appl. Phys.* **1990**, *28*, 542.